
$\gamma\delta$ T cell receptor recognition of CD1d in a lipid-independent manner

Received: 21 July 2025

Accepted: 5 December 2025

Michael T. Rice, Sachith D. Gunasinghe, Chhon Ling Sok, Mengqi Pan, Chan-Sien Lay, Benjamin S. Gully & Jamie Rossjohn

Cite this article as: Rice, M.T., Gunasinghe, S.D., Sok, C.L. *et al.* $\gamma\delta$ T cell receptor recognition of CD1d in a lipid-independent manner. *Nat Commun* (2025). <https://doi.org/10.1038/s41467-025-67653-0>

We are providing an unedited version of this manuscript to give early access to its findings. Before final publication, the manuscript will undergo further editing. Please note there may be errors present which affect the content, and all legal disclaimers apply.

If this paper is publishing under a Transparent Peer Review model then Peer Review reports will publish with the final article.

$\gamma\delta$ T cell receptor recognition of CD1d in a lipid-independent manner

Michael T. Rice¹, Sachith D. Gunasinghe^{1,¶}, Chhon Ling Sok¹, Mengqi Pan¹, Chan-Sien Lay¹, Benjamin S. Gully^{#1,¶} and Jamie Rossjohn^{#1,2}

¹ Infection and Immunity Program and Department of Biochemistry and Molecular Biology, Biomedicine Discovery Institute, Monash University, Clayton Victoria, Australia

² Institute of Infection and Immunity, Cardiff University School of Medicine, Heath Park Cardiff, CF14 4XN, United Kingdom

joint senior and corresponding authors: Ben.gully@monash.edu, Jamie.rossjohn@monash.edu

¶ Present address: Olivia Newton-John Cancer Research Institute, Heidelberg, VIC, Australia. School of Cancer Medicine, La Trobe University, Heidelberg, VIC, Australia.

Abstract

The monomorphic antigen-presenting molecule CD1d presents lipid antigens to both $\alpha\beta$ and $\gamma\delta$ T cells. While type I natural killer T cells (NKT) display exquisite specificity for CD1d presenting α -galactosylceramide (α -GalCer), the extent of lipid specificity exhibited by CD1d-restricted $\gamma\delta$ T cells remains unclear. Here, we demonstrate that human $\gamma\delta$ T cell receptors (TCRs) can recognise CD1d in either a lipid-dependent or lipid-independent manner with weak to moderate affinity. Using small-angle X-Ray scattering, we find that $\gamma\delta$ TCR-CD1d binding modality is conserved across distinct CD1d-restricted TCRs. In functional assays, CD1d $\gamma\delta$ TCR affinity was a poor predictor of $\gamma\delta$ T cell line activation. Moreover, CD1d presenting endogenous lipids was sufficient to stimulate T cell activation and induce $\gamma\delta$ TCR-CD3 clustering and phosphorylation in a dose-dependent manner. Elongation of the $\gamma\delta$ TCR-CD3 complex by the inclusion of the $C\gamma 2$ and $C\gamma 3$ - encoded constant domains perturbed cellular activation whilst maintaining the ability to form functional $\gamma\delta$ TCR clusters. The crystal structure of a $V\delta 1\gamma\delta^+$ TCR-CD1d complex showed that the $\gamma\delta$ TCR sat atop of the CD1d antigen-binding cleft but made no contacts with the presented lipid antigen. These findings provide a molecular basis for lipid-independent CD1d recognition by $\gamma\delta$ TCRs.

Introduction

The human adaptive immune compartment comprises of two lineages of T cells expressing heterodimeric T cell receptors (TCR), $\alpha\beta$ and $\gamma\delta$. $\gamma\delta$ T cells are a diverse population of unconventional lymphocytes that display broad effector functions of both adaptive and innate immune cells ¹. Unconventional $\alpha\beta$ T cells, such as mucosal associated invariant T cells and natural killer T cells (NKT) which recognise MR1 and CD1d respectively, have been described as innate-like due to their restricted TCR usage and rapid onset of effector functions ². $\gamma\delta$ T cells can display similar innate-like characteristics, exhibiting limited TCR diversity and eliciting effector functions via innate receptors ³. Conversely, clonal expansion of $\gamma\delta$ T cell clones in Merkel cell carcinoma, as well as malarial and cytomegalovirus infections has been observed, suggesting specific development of adaptive $\gamma\delta$ T cells ^{4, 5, 6}.

$\gamma\delta$ T cells subsets include $V\delta 1^+$ and $V\delta 2^+$ compartments that are highly abundant within peripheral tissues and peripheral blood, respectively. $V\delta 1^+$ $\gamma\delta$ T cells are enriched at epithelial sites

such as the gut, liver or lungs (5-10%) and present at low frequency within peripheral blood (<1%)^{7, 8, 9}. V δ 1 $^+$ γ δ T cells are an adaptive-like T cell population, with peripheral blood and tissue-resident V δ 1 $^+$ γ δ T cells undergoing clonal expansion from an initially diverse pool of TCR sequences accompanied by a phenotypic change^{7, 10}. Human and mouse intestinal mucosa contain γ δ intraepithelial lymphocytes (IELs) that rapidly mobilise upon infection to maintain barrier integrity^{11, 12}. However, the precise mechanism underpinning their function is complex, as their infection sensing and cytotoxic effector functions can occur in either a TCR-dependent or -independent manner^{11, 12}. It is clear, however, that there is a crosstalk between gut microbiota and γ δ T cells that serves to regulate cellular function^{11, 13}. Li and colleagues demonstrated that disruption of the microbiota by antibiotic treatment resulted in a significant reduction of the number of IL-17A producing hepatic γ δ T cells¹³. Retention of hepatic IL-17A $^+$ γ δ T cells was dependent upon CD1d lipid antigen presentation, as CD1d-deficient mice had a reduced IL-17A $^+$ γ δ T cell population akin to antibiotic-treated mice¹³.

In humans CD1d has been shown to present endogenous and exogenously-derived antigens to both peripheral blood and IEL V δ 1 $^+$ and V δ 3 $^+$ γ δ T cells^{14, 15, 16, 17, 18, 19}. CD1d and γ δ T cells are both enriched in barrier sites, such as the liver, indicating TCR recognition of CD1d is potentially involved in tissue γ δ T cell retention and cellular activation in humans^{8, 20}. Human CD1d-reactive γ δ T cells are primarily CD4 $^-$ CD8 $^-$, whilst the majority of type I α β NKT cells are CD4 $^+$ and, unlike the lipid-specific type I α β NKT cells, peripheral blood mononuclear cells (PBMC)-derived γ δ T cells from healthy donors recognise CD1d presenting an array of lipid antigens¹⁹. Structures of two V δ 1 $^+$ γ δ TCRs bound to CD1d revealed γ δ TCRs can make direct contacts to the presented lipid antigens^{18, 19}. Direct recognition of the presented antigen directly contrasts the recently resolved antigen-independent binding by MR1 and CD1a-reactive γ δ TCRs^{21, 22, 23}. Similarly, γ δ IELs produced more TNF- α in response to CD1d presenting endogenously derived lipids, rather than CD1d-sulfatide, raising questions on the requirement of lipid engagement to mediate γ δ T cell effector functions¹⁸. Previous tetramer staining and activation experiments on primary V δ 1 $^+$ γ δ $^+$ CD1d- α -GalCer $^+$ cells, suggested donor-specific patterns of lipid-independent and -dependent cell staining and CD1d dependent activation¹⁹.

Here, we characterise a panel of these previously identified CD1d- α -GalCer reactive V δ 1 $^+$ T cells to determine the extent to which V δ 1 $^+$ CD1d binding is lipid-dependant¹⁹. We report that

$\gamma\delta$ TCR recognition of CD1d is either unaltered or enhanced upon lipid engagement. Further, we determine the structure of a $\gamma\delta$ TCR recognising CD1d that binds at a site distal to the presented lipid antigen. We provide the molecular basis of CD1d lipid-independent recognition by a $\gamma\delta$ TCR.

Results

Affinity of $V\delta 1^+$ $\gamma\delta$ TCRs for CD1d presenting lipid antigens

To offer broad insight into $V\delta 1^+$ $\gamma\delta$ TCR recognition of CD1d, we used a panel of previously identified CD1d-reactive $\gamma\delta$ TCRs including diverse gene elements, $V\delta 1V\gamma 5^+$ (TCR2), $V\delta 1V\gamma 2^+$ (TCR3), $V\delta 1V\gamma 9^+$ (TCR6), $V\delta 1V\gamma 5^+$ (TCR7), $V\delta 1V\gamma 5^+$ (TCR8) (**Supplementary Table 1**)¹⁹. We recombinantly expressed and purified these $\gamma\delta$ TCRs alongside the control 9C2 $\gamma\delta$ TCR and the NKT.15 $\alpha\beta$ TCR^{19, 24}. We next conducted surface plasmon resonance (SPR) with immobilised CD1d loaded with α -GalCer (CD1d- α -GalCer), endogenously loaded lipids (CD1d-‘endo’) and CD1b-‘endo’. None of the $\gamma\delta$ TCRs tested here recognised CD1b-‘endo’ and specifically bound CD1d via two divergent patterns of specificity (**Supplementary Figure 1**). The $\gamma\delta$ TCRs 2, 3 and 6 bound to CD1d-‘endo’ ($K_D = 3.34 \pm 0.24 \mu M$, $K_D = 6.63 \pm 2.09 \mu M$, $K_D = 5.83 \pm 1.19 \mu M$) and CD1d- α -GalCer ($K_D = 3.70 \pm 0.33 \mu M$, $K_D = 3.09 \pm 0.74 \mu M$, $K_D = 5.08 \pm 0.98 \mu M$) with moderate affinity comparable to other $\gamma\delta$ TCR-MHC-I like interactions^{18, 21, 22, 23, 25} (**Figure 1A**). The lipid-independent recognition of CD1d by $\gamma\delta$ TCR 2, 3 and 6 contrasted with the NKT.15 $\alpha\beta$ TCR, which displayed high-affinity binding to CD1d- α -GalCer ($K_D = 0.44 \pm 0.04 \mu M$) and weak binding to CD1d-‘endo’. The apparent lipid cross-reactive $V\delta 1^+$ $\gamma\delta$ TCR CD1d binding observed here, has also been observed for CD1a and CD1b specific $\gamma\delta$ TCRs that displayed ‘lipid-agnostic’ binding^{21, 25}.

Comparatively, $\gamma\delta$ TCRs 7 and 8, weakly recognised CD1d-‘endo’ ($K_D = 36.89 \pm 8.34 \mu M$, $K_D = 53.68 \pm 3.85 \mu M$), yet bound CD1d- α -GalCer with higher affinity ($K_D = 13.84 \pm 2.62 \mu M$, $K_D = 14.19 \pm 2.72 \mu M$) suggesting co-recognition of CD1d and the presented lipid antigen. Lipid-modulated recognition of CD1d by $\gamma\delta$ TCRs has been observed by the 9C2 and DP10.7 $V\delta 1^+$ TCRs, which directly contacted the presented antigens via CDR3 γ and CDR3 δ loops respectively^{18, 19}. Our experiments suggest $\gamma\delta$ TCRs may recognise CD1d via two mechanisms potentially binding the presented lipid or solely recognising the CD1d molecule itself.

V δ 1 $^+$ $\gamma\delta$ TCRs recognise CD1d via similar binding modes

To identify whether the $\gamma\delta$ TCRs investigated here bound atop of CD1d or adopted more unusual ligand binding modes as seen in MR1 and CD1a reactive $\gamma\delta$ TCRs, we performed in-line size-exclusion chromatography coupled small angle X-ray scattering (SEC-SAXS) experiments (**Figure 1B**, **Supplementary Figure 2**)^{21, 22, 23}. The $\gamma\delta$ TCRs 7 and 8 co-complex samples were excluded from further analyses as the scattering profiles indicated a mixture of TCR and CD1d components and TCR dimers, rather than stable complexes in solution. The scattering profiles for the V γ 2 $\gamma\delta$ TCR3 and V γ 9 $\gamma\delta$ TCR6 were consistent with a globular protein. Compared with $\gamma\delta$ TCRs 3 and 6, the $\gamma\delta$ TCRs 2 and 8 scattering profiles were indicative of larger protein samples that suggested TCR dimerisation, with an oligomeric status of 1.8 and 1.5 respectively (**Supplementary Table 2**, **Supplementary Figure 2**). This appears to be a conserved feature with V γ 5 TCRs such as $\gamma\delta$ TCRs 2 and 8, corroborating previous SAXS, X-ray crystallography and cryo-EM experiments^{19, 23, 26, 27}. Evaluation of the scattering profiles by comparison to known macromolecular structures of a V γ 5 TCR and V γ 5 TCR dimer confirmed that the $\gamma\delta$ TCRs 2 and 8 formed a dimer in solution (**Supplementary Figure 3**). SAXS analyses of CD1d revealed scattering consistent with a globular monomer in solution.

Upon complexation with CD1d, $\gamma\delta$ TCRs 2, 3 and 6 shifted on SEC, indicative of complex formation (**Supplementary Figure 3C**). We next generated, aligned and averaged multiple *ab initio* reconstructions of the $\gamma\delta$ TCR 2, 3 and 6-CD1d-‘endo’ complex samples. The *ab initio* reconstructions revealed oblate particles that closely replicated the 9C2 $\gamma\delta$ TCR-CD1d complex, suggesting the endo-reactive $\gamma\delta$ TCRs 2, 3 and 6 recognised CD1d similarly to 9C2 (**Figure 1B**)¹⁹. To establish the $\gamma\delta$ TCR interaction mode for CD1d, we compared the measured scattering profiles with theoretical scattering profiles derived from known macromolecular structures of $\gamma\delta$ TCR-MHC-like complexes including the 9C2 $\gamma\delta$ TCR in complex with CD1d- α -GalCer structure^{28, 29, 30}. These analyses strongly supported an on top-docking geometry (Chi values), for $\gamma\delta$ TCRs 2, 3 and 6 as the scattering profiles closely matched the theoretical curve for 9C2 and a poor alignment of the G7 $\gamma\delta$ TCR-MR1 complex where the TCR docked underneath the antigen binding platform (**Supplementary Figure 3**)²³. Collectively, our SPR and SEC-SAXS

experiments revealed dual mechanisms for $\gamma\delta$ TCR recognition of CD1d, including lipid antigen-dependent or -independent means that adopt similar ‘end-to-end’ docking modes.

CD1d-mediated V δ 1 $^+$ $\gamma\delta$ T cell activation

To assess whether lipid antigen-dependent or -independent mechanisms for CD1d reactivity contributed to differing cellular activation outcomes we transduced the V δ 1 $^+$ $\gamma\delta$ TCRs into a Jurkat.76 (J76) reporter cell line and assessed T cell activation by CD69 upregulation and CD3 downregulation. We compared $\gamma\delta$ TCR signalling to the 9C1 $\alpha\beta$ TCR, as it adopts a similar orthogonal binding mode atop CD1d as other previously known CD1d restricted $\gamma\delta$ TCRs³¹. In the absence of lipid pulsing, all V δ 1 $^+$ $\gamma\delta$ TCRs upregulated CD69 in response to CD1d expressing K-562 lymphoblast cells although to differing extents but did not respond to wildtype K-562 cells (**Figure 2A**) (**Supplementary Figure 9A**). The $\gamma\delta$ TCRs 2, 3, 7 and 8 expressing J76 cells upregulated CD69 following CD1d stimulation without a specific lipid antigen, whereas $\gamma\delta$ TCR 6 although statistically significant did not appreciably upregulate CD69 compared to the other $\gamma\delta$ TCRs, which mirrored negligible CD3 downregulation following CD1d stimulation. Whereas CD3 down-regulation was observed for the $\gamma\delta$ TCRs 2, 3, 7 and 8 expressing J76 cells suggesting immune synapse formation following CD1d stimulation. We next probed whether α -GalCer treatment impacted V δ 1 $^+$ $\gamma\delta$ T cell activation, which yielded no major alteration in activation (**Figure 2B**). In comparison, the lipid-specific 9C1 $\alpha\beta$ TCR upregulated CD69 at even the lowest concentration of α -GalCer, with a dose-dependent increase (**Figure 2B**) (**Supplementary Figure 9B**). To further investigate the divergence between our steady-state affinity measurements and T cell stimulation capacity, we investigated the temporal impact of T cell signalling as noted to effect MR1-reactive $\gamma\delta$ T cell activation³². We measured $\gamma\delta$ TCR expressing J76 cell activation by detecting Nur77 upregulation after 2 hours of stimulation with CD1d expressing K-562 cells. Here $\gamma\delta$ TCR 2 and 3 had the highest frequency of Nur77 $^+$ cells, followed by $\gamma\delta$ TCRs 7 and 8 which were comparable to the well characterised 9C2 $\gamma\delta$ TCR (**Figure 2C**) (**Supplementary Figure 10**). $\gamma\delta$ TCR 6, which had the lowest level of CD69 upregulation, also failed to upregulate Nur77 despite specific TCR reactivity to CD1d as attested by SPR. This may stem from some $\gamma\delta$ TCRs requiring high antigen levels to trigger cellular activation³². Further, TCR-ligand affinity may influence $\gamma\delta$ TCR signalling outcomes, as the highest affinity $\gamma\delta$ TCRs 2 and 3 had the highest

frequency of Nur77⁺ cells and CD3 downregulation. Collectively, these experiments indicated that the V δ 1⁺ TCR panel activated in response to CD1d-expressing cells independently of a specific lipid antigen, suggesting a disconnect between steady-state affinity and T cell activation capacity.

CD1d-induced $\gamma\delta$ TCR clustering

To identify whether differences in T cell activation were associated with with $\gamma\delta$ TCR-CD3 triggering and proximal signalling events, we performed single-molecule imaging with CD1d-endo and CD1d- α -GalCer using a supported lipid bilayer system (**Figure 3A and B**). In response to CD1d-endo, of the $\gamma\delta$ TCRs we investigated only $\gamma\delta$ TCR-6 failed to undergo significant changes to TCR cluster number, cluster area or percentage of TCR localisations compared to unstimulated ICAM-1 alone (**Figure 3C and Supplementary Figure 4**). This mirrored our CD69 and Nur77 experiments, where $\gamma\delta$ TCR-6 was weakly reactive to CD1d. Indeed, following activation the $\gamma\delta$ TCRs 2, 3, 7 and 8, underwent the greatest extent of TCR clustering across both concentrations of CD1d-endo tested. Notably, all $\gamma\delta$ TCR cell lines tested showed increased TCR cluster area and enhanced TCR triggering, with increased CD1d ligand abundance, a feature also noted with a MR1 reactive $\gamma\delta$ TCR³². As SPR indicated that $\gamma\delta$ TCR7 and 8 had a higher affinity for CD1d- α -GalCer compared to CD1d-endo, we tested CD1d- α -GalCer effects on $\gamma\delta$ TCR clustering and proximal signalling (**Figure 3B and D**). As a control we included the 9C1 $\alpha\beta$ TCR, which underwent TCR clustering upon engagement with CD1d- α -GalCer, but not CD1d-endo or ICAM-1 (**Figure 3C and D**). Again, we observed increased TCR clustering with increasing amounts of CD1d- α -GalCer (**Figure 3D and Supplementary Figure 4B**). Across all cell lines, apart from $\gamma\delta$ TCR 7, there was an increase in activated TCR clustering with CD1d- α -GalCer compared to CD1d-endo. Collectively our single-molecule imaging experiments show that CD1d-endo is sufficient to induce $\gamma\delta$ TCR clustering and phosphorylation, although TCR triggering was enhanced with higher-affinity lipid antigens and increasing antigen concentrations. The remarkable flexibility of the $\gamma\delta$ TCR-CD3 signalling apparatus may require higher CD1d ligand densities to stabilise the complex and promote TCR signalling across shorter time points as seen with MR1 reactive $\gamma\delta$ TCRs³².

Impact of C γ Exon insertions on $\gamma\delta$ T cell activation

Further complicating our understanding of $\gamma\delta$ TCR triggering is allelic variants of the $\gamma\delta$ TCR constant domain. The TCR γ locus encodes two constant region genes, a *Trgc1* ($C\gamma 1$) which consists of three exons, and a *Trgc2* gene that contains 4, or rarely five exons stemming from exon 2 duplications and triplications, respectively³³. The duplication and triplication events of exon 2 result in a 16 and 32 amino acid extension of the $\gamma\delta$ TCR connecting peptide and a C>W mutation that prevents disulfide formation with C δ . Extended connecting peptides were recently shown to endow the $\gamma\delta$ TCR with extreme dynamism within the CD3 signalling apparatus, which in turn modulated proximal signalling^{26, 32}. Xin et al. recently demonstrated that in the exon 2 duplication event $C\gamma 2$, dampened $\gamma\delta$ TCR activation compared to the $C\gamma 1$ ²⁶. We investigated whether the exon 2 triplication event, $C\gamma 3$, had a further impact on $\gamma\delta$ TCR signalling outcomes, using the previously well characterised CD1d restricted 9C2 $\gamma\delta$ TCR^{19, 26}. Following stimulation by CD1d K-562 cells, the $C\gamma 1$ allele led to the greatest CD69 upregulation, with a marked reduction in CD69 production by the $C\gamma 2$ allele (**Figure 4A**) (**Supplementary Figure 11A**). The $C\gamma 3$ allele completely inhibited $\gamma\delta$ T cell activation, as it did not upregulate CD69 above baseline levels. As the 9C2 $\gamma\delta$ TCR has improved affinity for CD1d presenting α -GalCer ($K_D = 16\mu M$) compared to CD1d-‘endo’ ($K_D = 35\mu M$), we reasoned that the antigen may serve to stabilise TCR-CD1d interactions leading to improved signalling outcomes¹⁹. While α -GalCer increased CD69 upregulation with 9C2 $C\gamma 1$, it did not improve signalling with either $C\gamma 2$ or $C\gamma 3$ (**Figure 4B**) (**Supplementary Figure 11B**). Therefore, elongation of the $\gamma\delta$ TCR-CD3 complex via $C\gamma$ Exon 2 duplication and triplication events, reduced and even ablated T cell activation. This raised questions on whether the $C\gamma 2$ and $C\gamma 3$ alleles could form functional $\gamma\delta$ TCR signalling complexes.

To address this, we performed single-molecule imaging on the 9C2 $C\gamma$ alleles (**Figure 4C**). Although $C\gamma 2$ and $C\gamma 3$ displayed reduced capacity to upregulate CD69 compared to $C\gamma 1$, both readily formed functional, similarly sized, TCR clusters against CD1d-endo and CD1d- α -GalCer indicating the $C\gamma$ exon duplication and triplications do not prevent TCR triggering (**Figure 4C-E** and **Supplementary Figure 5**). Instead, the exon 2 insertions may increase the length and flexibility of the membrane proximal connecting peptides that link the $\gamma\delta$ TCR extracellular domains to the CD3 signalling apparatus. This may limit efficient TCR signal transduction and ultimately cellular activation, corroborating evidence that $\gamma\delta$ TCR flexibility and connecting peptide length impact $\gamma\delta$ T cell activation^{26, 32}. Additionally, $\gamma\delta$ TCR docking modalities are

thought to be critical for functional $\gamma\delta$ TCR signalling²³. Yet, how $\gamma\delta$ TCRs engage their ligands remains largely unclear and can vary dramatically across the same ligand^{22, 23}.

Overview of the $\gamma\delta$ TCR 2 CD1d-‘endo’ complex

To gain insight into the molecular basis of $\gamma\delta$ TCR CD1d lipid-independence we determined the X-ray crystal structure of $\gamma\delta$ TCR 2 bound to CD1d-‘endo’ (**Supplementary Table 3**). Although we determined the structure of the $\gamma\delta$ TCR-CD1d complex with CD1d carrying a mixture of endogenous lipids from the mammalian expression system, density was observed within the antigen presenting cleft of CD1d indicating the abundance of one class of lipid antigen. Here, we modelled sphingomyelin which has previously been identified as a component of the CD1d-‘endo’ lipid repertoire (**Supplementary Figure 6A and B**)^{34, 35}. Despite sphingomyelin being modelled into the crystal structure, we cannot exclude the possibility our crystal structure likely contains a mixture of phospholipid antigens.

The $\gamma\delta$ TCR 2 docked over the extreme A’ end of CD1d antigen-binding cleft (**Figure 5A**). This docking geometry was similar to the 9C2 $\gamma\delta$ TCR, which shares the same V δ 1V γ 5 TCR chain usage, that bound over the A’ of CD1d (**Figure 5B, E and H**), and distinct to the V δ 1V γ 4 DP10.7 $\gamma\delta$ TCR which bound centrally over the protruding sulfatide lipid head group (**Figure 5C, F and I**). The $\gamma\delta$ TCR 2 bound orthogonally atop CD1d (~80°), with the V γ and V δ chains positioned centrally over the α 1 and α 2 helices, respectively (**Figure 5D and G**).

This more ‘conventional’ $\gamma\delta$ TCR 2 recognition mode differed from the perpendicular, side and underneath docking observed for the recently resolved MR1 and CD1a $\gamma\delta$ TCR complex structures^{21, 22, 23}. However, the extreme A’ binding mode was unusual, with the V δ /V γ shifting 10Å/6Å in respect to the 9C2 TCR and 23Å/26Å compared to the DP10.7 $\gamma\delta$ TCR (**Supplementary Figure 6C**). Thus, the CDR loop positions and molecular contacts of the $\gamma\delta$ TCR 2 to CD1d are unique to this complex, and different to other $\gamma\delta$ TCR and $\alpha\beta$ TCR-CD1d complexes. The CD1d- $\gamma\delta$ TCR 2 complex further demonstrates the diversity of $\gamma\delta$ TCR antigen recognition even across $\gamma\delta$ TCRs with the same gene usage.

$\gamma\delta$ TCR 2 binds CD1d independently of lipid antigens

The total buried surface area (BSA) of the TCR-CD1d interface was $\approx 1860\text{\AA}$ (**Figure 6A**). The TCR chains contributed asymmetrically to the interface with $\approx 59\%$ of the interface mediated by TCR- γ and $\approx 41\%$ by TCR- δ (**Figure 6A**). This contrasts with the emerging trend of V $\delta 2\cdot\gamma\delta$ TCR-ligand recognition being dominated by the TCR- δ chain, in particular CDR3 δ ^{36, 37}.

Notably, FW γ contributed to this interface with several polar interactions to CD1d (**Figure 6B**) (**Supplementary Table 4**). This served to stabilise CDR1 γ and CDR2 γ , which were positioned either side of the CD1d- $\alpha 1$ helices and made a number of key contacts to CD1d (**Figure 6B**).

A key determinant in lipid binding for the 9C2 V $\delta 1\cdot V\gamma 5$ TCR was CDR3 γ , namely Arg103 γ and Tyr11 γ that directly contact the head-group of α -GalCer. Instead, the CDR3 γ of $\gamma\delta$ TCR 2 did not contact the lipid antigen (**Figure 6C**), providing the molecular basis for the lipid-independent binding identified in the SPR experiments. Rather CDR3 γ solely contacted the CD1d molecule itself (**Figure 6C**). The 9C2 TCR and $\gamma\delta$ TCR2 possess different CDR3 γ loop lengths, 18 versus 13 amino acids, which may account for the differences identified in biochemical and structural based observations. The shorter CDR3 γ loop of $\gamma\delta$ TCR 2 leads to a rearrangement of the TCR-CD1d interface compared to the 9C2 TCR, shifting the CDR3 γ/δ loops $\sim 8\text{\AA}$ towards the A' of CD1d, preventing direction recognition of the presented lipid antigen.

TCR- δ chain binding was predominately mediated by the CDR3 δ loop. CDR2 δ did not contact CD1d while CDR1 δ made minimal contacts, a feature not seen in other CD1d- $\gamma\delta$ TCR complexes that relied heavily on CDR1 δ for CD1d engagement^{18, 19}. Central to this recognition was Trp99 δ , which wedged in-between the α helices of CD1d, forming an extensive network of interactions with CD1d (**Figure 6D**). Similar to CDR3 γ , the CDR3 δ loop of $\gamma\delta$ TCR-2 is shorter compared to 9C2, 12 vs 16 amino acids. Consequently, neither CDR3 γ or CDR3 δ made contacts to the presented lipid antigen providing structural evidence for lipid independent CD1d binding by a $\gamma\delta$ TCR.

A conserved aromatic zone on CD1d

$\gamma\delta$ TCR 2 docking atop CD1d was reminiscent of a single domain antibody (VHH) 1D12 which also bound over the A' distal end of CD1d and make no contacts to the presented lipid antigen³⁸. VHH1D12 bound with extremely high nanomolar affinity and served to stabilise NKT TCR binding to CD1d promoting cellular activation. Akin to Trp99 δ of the $\gamma\delta$ TCR 2, Phe29 from

VHH1D12-CDR1 served as a lynchpin of binding, interacting with Phe58, Gln62, Trp160 Thr165 and Gln168, which were all binding partners with Trp99 δ (**Supplementary Figure 7A and B**). We then analysed other $\gamma\delta$ and atypical $\alpha\beta$ NKT CD1d-TCR complexes that similarly bound over the A' end of CD1d to determine whether this aromatic zone was a conserved binding motif. Indeed, CDR1 δ of both the $\gamma\delta$ 9C2 and 9B4 $\delta/\alpha\beta$ TCRs bound the same motif as CDR3 δ of $\gamma\delta$ TCR 2, suggesting recognition of this motif serves as a key determinant of TCR-ligation (**Supplementary Figure 7C and D**). Although the CDR1 δ of DP10.7 TCR was shifted more centrally, it was pincerred by Trp153 and Trp160, providing further evidence aromatic interactions are central to $\gamma\delta$ TCR recognition of CD1d (**Supplementary Figure 7E**). The atypical $\alpha\beta$ NKT TCRs, 9C1 and 9B2 similarly interacted with the A' of CD1d, with Phe111 of CDR3 α and CDR3 β of 9C1 and 9B2, respectively, interacting with Trp160 of CD1d (**Supplementary Figure 7F and G**). This suggests the A' of CD1d containing a large non-polar patch, serves as a key TCR binding site for atypical $\alpha\beta$ NKT and $\gamma\delta$ TCRs that is primarily governed by CDR loops containing aromatic residues (**Supplementary Figure 7H**)³¹.

Discussion

Here, we provide further evidence that $\gamma\delta$ TCRs adopt diverse antigen recognition strategies³⁷, either recognising the CD1d molecule itself or binding both CD1d and the lipid antigen. The V δ 1-V γ 5 TCRs investigated here displayed two modes of interaction being CD1d-endo reactive ($\gamma\delta$ TCR-2) or displayed a lipid-modulated interaction ($\gamma\delta$ TCR-7 and 8) indicating that $\gamma\delta$ TCR recognition strategies are potentially clonally dependent. Although $\gamma\delta$ TCR clonal expansion has been identified whether this occurs in an MHC-I-like dependent manner remains unclear^{7, 10}.

The recent elucidation of the $\gamma\delta$ TCR-CD3 complex via cryo-EM, highlighted the flexibility of the $\gamma\delta$ TCR ectodomain within the signalling apparatus, was resolved as consequence of V γ 5 chain dimerization which stabilised the TCR ectodomain^{26, 32}. In our SEC-SAXS experiments we noted dimerization of two V δ 1-V γ 5 TCRs, a feature that was absent in V γ 9 and V γ 2 V δ 1 $^+$ TCRs. Mutagenesis of the dimerization interface in the 9C2 $\gamma\delta$ TCR ablates antigen driven CD69 $^+$ upregulation despite the TCR-CD3 complex maintaining its functionality²⁶. One potential explanation is that V γ 5 $^+$ TCRs dimerise to promote TCR mediated signalling in the

absence of high-affinity ligand interactions. Hypo-reactive $\gamma\delta$ TCRs are a recurring theme, with $\gamma\delta$ TCRs reactive towards MR1 and CD1a being poor activators despite binding their ligands with moderate affinity^{21, 23}. Whether such phenomena occur in primary $\gamma\delta$ T cells is unclear but raises further questions on the mechanisms underpinning $\gamma\delta$ TCR triggering, particularly if other V γ pairings induce dimerization to enhance TCR signal propagation.

Similar to MR1-, CD1b- and CD1a-reactive $\gamma\delta$ T cells, CD1d-restricted $\gamma\delta$ T cells activated in the absence of lipid antigen stimulation, suggesting CD1d ligand availability is a regulator of $\gamma\delta$ T cell activation^{21, 23, 25, 32}. A limitation of this study is the use of Jurkat T cells to investigate $\gamma\delta$ T cell activation raising questions on whether our conclusions extend to primary $\gamma\delta$ T cells. We have previously demonstrated that PBMC derived CD1d-restricted $\gamma\delta$ T cells activate in response to cells over-expressing CD1d in the absence of lipid pulsing¹⁹. This alludes to CD1d-restricted primary $\gamma\delta$ T cell activation also being dependent on ligand availability although further experiments are required to confirm these preliminary findings.

Ligand availability limiting $\gamma\delta$ T cell activation is potentially resultant of the increased flexibility of the $\gamma\delta$ TCR within the $\gamma\delta$ TCR-CD3 signalling complex, therefore increasing the number of ligand interactions required to stabilise the $\gamma\delta$ TCR-CD3 complex to promote signal transduction^{26, 32}. The C γ alleles further add to this flexibility, but do not impede TCR ligand binding²⁶. However, increasing the length of the $\gamma\delta$ TCR-CD3 complex via the C γ 2 and C γ 3 alleles, reduced and impeded cellular activation respectively, despite maintaining their ability to form competent $\gamma\delta$ TCR-CD3 complexes. This further highlights how in isolation, $\gamma\delta$ TCR ligand affinity is a poor predictor for $\gamma\delta$ T cell functional outcomes, as $\gamma\delta$ TCR flexibility and ligand binding modes have also been shown to regulate $\gamma\delta$ T cell activation^{21, 23, 26, 32}.

We next determined the structure of a V δ 1-V γ 5 TCR bound to CD1d-‘endo’. The $\gamma\delta$ TCR2 was situated over the A’ roof of CD1d that resulted in the absence of $\gamma\delta$ TCR-lipid interactions. This extends an emerging theme of $\gamma\delta$ TCRs displaying antibody-like ligand recognition^{21, 22, 23}.

The A’ lipid-independent docking by $\gamma\delta$ TCR-2 was similar to the BK6 and 3C8 $\alpha\beta$ TCRs which bound CD1a and CD1c, respectively^{39, 40}. Whilst both BK6 and 3C8 bound the A’ roof of CD1a/c, neither $\alpha\beta$ TCR contacted the presented lipid antigens, diverging from the CD1-lipid co-recognition paradigm^{39, 40}. In the absence of direct lipid interactions, presentation of ‘non-permissive’ lipids that disrupt TCR-CD1 binding serve to regulate $\alpha\beta$ T cell activation⁴¹.

Divergence from the co-recognition model has recently been observed in type I NKT cells, that recognised small headless ceramide lipids presented by CD1d⁴². Primarily recognising CD1d, the limited contacts of the NKT TCR to the presented ceramide coincided with reduced cellular staining and activation compared to the prototypic α -GalCer antigen. Deciphering whether $\gamma\delta$ T cells will recognise antigens in a similar lipid-reactive or co-recognition dependent manner is unpredictable. For instance, V δ 1 $^+$ TCR complexes display remarkable diversity in binding modalities. The V δ 1 $^+$ $\gamma\delta$ TCR-2-CD1d complex determined here, continues the trend of breaking the co-recognition paradigm as seen in MR1 and CD1a TCR-ligand complexes, and differs from the 9C2 and DP10.7 $\gamma\delta$ TCRs that co-recognise the presented lipid antigen and CD1d molecule^{18, 19, 21, 22, 23}.

Our findings illustrate that $\gamma\delta$ TCRs can recognise CD1d via diverse mechanisms and bind irrespective of the lipid antigen. This represents the structural characterisation of a $\gamma\delta$ TCR bound to CD1d in an lipid-independent manner. This further illuminates the complexity in understanding $\gamma\delta$ T cell activation and their roles within the immune response more broadly.

Methods

Protein Production and Purification

The $\gamma\delta$ TCRs and CD1d constructs were designed and expressed in Human Embryonic Kidney (HEK) 293F cells (Gibco) and purified as previously described¹⁹. Both $\gamma\delta$ TCR and CD1d constructs contained C-terminal His-Tags, Fos-Jun Zippers and a BirA sequence. In brief, HEK-293F cells were transfected with either CD1d- β 2M or TCR- γ and TCR- δ chains and allowed to express for 5 days at 37°C, 5% CO₂. On days 1 and 3, media was supplemented with 1mM NEAA, 1mM GlutaMAX and 33mM Glucose. On day 5, the transfected culture was harvested, centrifuged at 4,000g at 4°C and the supernatant dialysed against 10mM Tris-HCl pH 8.5, 300mM NaCl. The dialysed samples were then purified via Ni-NTA, followed by size exclusion chromatography to yield homogenous pure protein. Prior to biochemical or crystallography-based experiments, the C-terminal His-tag and Fos-Jun zippers were removed by thrombin digestion and the protein further resolved by size exclusion chromatography. For surface plasmon resonance experiments, CD1d- β 2M was expressed in High-Five insect cells (maintained in house >10 years), purified and

biotinylated as previously described⁴³. The $\alpha\beta$ NKT.15 TCR was expressed in bacterial cells, refolded and purified as previously described⁴³.

Crystallisation and Structural Analysis

Prior to crystallisation, HEK-293F Gnti-/- produced $\gamma\delta$ TCR 2 and CD1d-‘endo’ were incubated overnight at 4°C at 1:1 molar ratio in the presence of EndoH (New England Biolabs). To resolve co-complexes from individual components SEC was performed via a SE 200 10/30 (GE Healthcare). Co-complexed fractions were pooled and concentrated to 8mg/mL for crystallisation experiments at the Monash Molecular Crystallisation Platform. Crystals of the $\gamma\delta$ TCR-2-CD1d-‘endo’ complex formed in 16% PEG 3350, 0.05 M CBTP pH 5.0. Individual crystals were cryoprotected in mother liquor with the addition of 40% PEG 400 and flash frozen. Data was collected on the MX2 beamline at the Australian Synchrotron⁴⁴. Data were processed using XDS and CCP programme suites. Molecular replacement was performed using Phenix⁴⁵, with the individual components of the $\gamma\delta$ TCR with the CDR loops removed in COOT (PDB ID: 4LHF) and CD1d- β 2M with the lipid antigen removed (PDB ID: 8SOS) were used as individual search models⁴⁶. A single $\gamma\delta$ TCR-CD1d complex was present in the asymmetric unit. Manual model building was performed in COOT and further refined in Phenix. Buried surface area was calculated by PDBePISA and molecular interactions analysed via CONTACT from the CPP4 Software Suite⁴⁷. The $\gamma\delta$ TCR 2-CD1d complex was refined and deposited in the Protein Data Base for structural validation.

Surface Plasmon Resonance

Surface plasmon resonance (SPR) experiments were performed on a BIACore T3000 ($\gamma\delta$ TCRs - 2, 7 and 8) and T200 ($\gamma\delta$ TCRs - 3 and 6) in TBS Buffer (10mM Tris-HCl pH 8.0, 150mM NaCl) with 0.5% bovine serum albumin (BSA) at 25°C. The $\alpha\beta$ NKT TCR, NKT.15 was used as a positive control for all SPR experiments. Biotinylated CD1d and CD1b proteins were coupled to a streptavidin chip (GE Healthcare) to approximately 1000-2000 response units (RU). Mammalian expressed $\gamma\delta$ and refolded $\alpha\beta$ NKT TCRs were used as the analyte and serially diluted from 200 to 0 μ M. Sensograms and TCR affinity curves were generated and analysed in GraphPad Prism 10. Experiments were performed twice with duplicate injections.

Size-Exclusion Chromatography small-angle X-ray scattering (SEC-SAXS) data collection

SEC-SAXS experiments were performed on the SAXs/WAXs beamline at the Australian Synchrotron with co-flow to minimise radiation damage and an in-line SEC⁴⁸. Prior to the SEC-SAXS experiment, $\gamma\delta$ TCRs and CD1d were incubated overnight at 4°C at 1:1 molar ratio. Approximately 60 μ L of each sample ranging from 5-10mg/mL were injected onto a Superose_6 5/150 increase column (GE Healthcare), in 10mM Tris-HCl pH 8.0, 150mM NaCl. SEC-SAXS images were analysed in BioXTAS RAW³⁰. Prior to analysis, images were buffer subtracted and to aid *ab initio* model interpretation only images containing co-complexed samples, as determined by Radius of Gyration (Rg) and Porod Volume (V_P), were kept for further analysis. In BioXTAS RAW, the raw scattering SEC-SAXS scattering curves, Guinier analysis, P(r) distribution plots, Rg and maximum particle dimension (Dmax) were determined. A summary of the SEC-SAXS data collection can be found in **Supplementary Figure S1** and **Supplementary Table S1**. *Ab initio* models were generated utilising DAMMIF in BioXTAS RAW, 15 reconstructions were generated, averaged and refined via DAMAVER and DAMMIN. X-ray crystallography structures were aligned to the generated reconstruction. CRYSTAL was then performed to compare the theoretical scattering from the aligned model to the raw scattering curves⁴⁹.

Generation of stable TCR cell lines

$\gamma\delta$ and $\alpha\beta$ TCRs were cloned into pMIG-II (pMSCV-IRES-GFP II), with the individual TCR chains separated by a P2A linker. Parental Jurkat-76 cells (maintained in house >10 years), which lack endogenous $\alpha\beta$ TCR expression and consequently CD3 cell surface expression, were retrovirally transduced with either $\gamma\delta$ or $\alpha\beta$ TCR genes. Jurkat-76 cells were maintained in RPMI supplemented with 10% FCS, 15mM HEPES, 1mM Sodium Pyruvate, 1x Non-essential amino acids and 2mM GlutaMax at 37°C at 5% CO₂ (all sourced from ThermoFisher). After 2 rounds of transduction, successful TCR transduction was assessed via Flowcytometry by the presence of GFP+ and staining of CD3+, α -CD3-PE (BD Biosciences, 1:200, #555333), cells. Multiple rounds of cell sorting were performed at the Monash FlowCore Facility, to attain a homogeneous GFP⁺ CD3⁺ cell population.

T cell activation Assays

T cell activation was assessed via the upregulation of CD69 and the downregulation of CD3, and Nur77 expression. For CD69 upregulation detection experiments, transduced Jurkat.76 cells were co-incubated with K562 cells for 16 hours at 37°C. The co-culture was then harvested, washed in PBS and stained with Zombie Aqua Live/Dead Stain (BioLegend). Cells were then washed with FACS Buffer and stained with α -CD1d-R710 (BD Biosciences, 1:200, #567984), α -CD3-PE (BD Biosciences, 1:200, #555333) and α -CD69-APC (BD Biosciences, 1:200, #555533) antibodies. For Nur77 experiments, transduced Jurkat.76 cells were incubated with K562 cells for 2 hours at 37°C and then harvested. Cells were then stained with Live/Dead stain and stained with α -CD1d-R710 (BD Biosciences, 1:200, #567984) and α -CD3-PE (BD Biosciences, 1:200, #555333). After washing with FACS buffer, cells were resuspended and incubated in Fixation Buffer in the dark at room temperature. Cells were then permeabilised and stained with α -Nur77-AF647 (BD Biosciences, 1:200, #566735). CD69 and Nur77 upregulation was then assessed at the Monash FlowCore Facility on a BD Fortessa, cells were gated on Lymphocytes, Single cells, Live cells, CD1d⁻ and CD3/GFP⁺. In GraphPad Prism v10, statistical analysis was performed via one-way ANOVA. Exact P-values are shown for all statistically significant comparisons; non-significant comparisons are not shown. Error bars denote S.E.M.

Preparation of Supported Lipid Bilayer (SLB)

Glass coverslips (0.17 mm thickness) were cleaned with 1 M KOH, rinsed with Milli-Q water, and dried in a fume hood after ethanol treatment. Following plasma cleaning, coverslips were attached to eight-well silicon chambers (ibidi, #80841). SLBs were prepared using vesicle extrusion of a 1 mg/ml liposome solution. The liposome composition included 96.5% DOPC, 2% DGS-NTA(Ni), 1% Biotinyl-Cap-PE, and 0.5% PEG5000-PE (mol%; Avanti Polar Lipids). Extruded liposomes were added to chambers (1:5 ratio with Milli-Q water containing 10 mM CaCl₂) and incubated for 30 min at room temperature before gentle PBS rinsing. Fluorescence recovery after photobleaching (FRAP) was used to examine SLB lateral mobility. Excess Ca²⁺ ions were removed with 0.5 mM EDTA, followed by Milli-Q water rinsing. NTA groups were recharged with 1 mM NiCl₂ solution for 15 minutes, followed by PBS washing.

Stimulation and Immunostaining of T cells on SLB

Biotinylated SLBs were coupled with streptavidin (100 µg/ml) followed by biotinylated CD1d- α -GalCer or CD1d-endo (1-10 nM). NTA-functionalized lipids were coupled with His-tagged ICAM-1 (200 ng/ml). SLBs were rinsed and pre-incubated with warm RPMI medium. Jurkat TCR transductants were stimulated on SLBs for 5 min at 37°C, fixed with 4% paraformaldehyde, permeabilized with 0.1% Triton X-100, and blocked with 5% BSA. Cells were immunostained with specific antibodies, namely anti-CD3 ε -Alexa Fluor 647 (BioLegend, #300416, Clone UCHT1) (1:300 dilution) and anti-pCD3 ζ -Alexa Fluor 568 (BD Biosciences, #558402) (1:300 dilution) for 1 hour at room temperature. After washing, a final fixation step was performed, and 0.1 µm TetraSpeck microspheres were embedded for drift correction during *d*STORM imaging.

Single-molecule Imaging with *d*STORM

Single-molecule localisation microscopy technique *d*STORM imaging was performed using a TIRF microscope (Nikon N-STORM 5.0) with a 100x oil immersion objective and multiple lasers. The imaging buffer contained TN buffer (50 mM Tris-HCl pH 8.0, 10 mM NaCl), GLOX oxygen scavenger system [0.5 mg/ml glucose oxidase (Sigma- Aldrich, #G2133); 40 mg/ml catalase (Sigma- Aldrich, #C-100); and 10% w/v glucose], and 10 mM 2-aminoethanethiol (MEA; Sigma- Aldrich, #M6500). Image sequences for *d*STORM were acquired on a total internal reflection fluorescence (TIRF) microscope (Nikon N-STORM 5.0) equipped with a 100x (1.49 NA) oil immersion objective and lasers (405 nm, 473 nm, 561 nm and 640 nm). Time series of 10,000 frames were acquired per sample, per channel (640 or 561 nm laser channel with continuous low-power 405 nm illumination) with an exposure time of 30 ms in TIRF mode. For dual-colour acquisition, higher wavelength channel (640 nm laser for Alexa Fluor 647) was acquired first, followed by the channel with shorter wavelength (561 nm laser for Alexa Fluor 568) using a sCMOS camera (Hamamatsu Orca-Flash 4.0 V3). Image processing, including fiducial markers-based drift correction, two-channel alignment, and generation of x-y particle coordinates for each localization was carried out by NIS-Elements AR software (version 5.2).

Cluster Analysis of Single-molecule Images

The degree of TCR clustering was quantified by using a custom-built DBSCAN algorithm implemented in MATLAB. Pre-determined parameters included minimum number of neighbours (3) and radius (20 nm). Clus-DoC analysis was performed to quantify spatial distribution and

colocalization of two proteins, in this case CD3 ϵ and pCD3 ζ . Density gradients were generated for each localization and normalized. Spearman correlation was used to calculate the rank correlation coefficient. DoC scores ranged from +1 (colocalization) to -1 (segregation), with 0 indicating random distribution. The DoC threshold for colocalization was set to ≥ 0.1 . One-way ANOVA with Tukey's multiple comparison was performed in GraphPad Prism v10. Statistical significance is denoted by asterisks with, * $P\leq 0.05$, ** $P\leq 0.01$, *** $P\leq 0.001$ and **** $P\leq 0.0001$, non-significant comparisons are not shown. Error bars denote S.E.M.

Data Availability

The $\gamma\delta$ TCR 2-CD1d complex structure is available on the Protein Database under the accession code, 9OX4 [<https://doi.org/10.2210/pdb9O4X/pdb>]. Data generated for this study is present in the article and supplementary material. Source Data are provided with this paper.

Code availability

Code for the cluster analysis algorithm can be found at (<https://github.com/PRNicovich/ClusDoC>).

Acknowledgements

This research was undertaken using the BioSAXS, SAXS/WAXS and MX2 beamlines at the Australian Synchrotron, part of the Australian Nuclear Science and Technology Organisation, and made use of the Australian Cancer Research Foundation detector. We thank Dr Ashish Sethi and the staff at the Australian Synchrotron for their assistance with data collection. We thank the staff from the Monash FlowCore, Monash Molecular Crystallisation Platform and Micromon facilities for their assistance. We thank Dr. Adam Uldrich for providing the 9C1 $\alpha\beta$ TCR pMIG-II plasmid. M.T.R was supported by an Australian Institute of Nuclear Science and Engineering Early Career Researcher Grant and a Faculty of Medicine Nursing and Health Sciences Early Career Postdoctoral Fellowship. S.D.G would like to thank staff at the Centre for Dynamic Imaging at Walter and Eliza Hall Institute of Medical Research for providing access to Single-Molecule Imaging microscope.

Author contributions

MTR - 1st author, collected, analysed data, wrote paper. SDG, single molecule imaging analyses. CSL, MP, CSL – undertook experiments/analysed experiments, revised the paper - JR & BSG – co-supervised project, co-wrote and revised paper, JR – project funding.

Conflicts of interest

The authors declare no conflicts of interest.

References

1. Vantourout P, Hayday A. Six-of-the-best: unique contributions of gammadelta T cells to immunology. *Nat Rev Immunol* **13**, 88-100 (2013).
2. Godfrey DI, Uldrich AP, McCluskey J, Rossjohn J, Moody DB. The burgeoning family of unconventional T cells. *Nat Immunol* **16**, 1114-1123 (2015).
3. de Vries NL, *et al.* gammadelta T cells are effectors of immunotherapy in cancers with HLA class I defects. *Nature* **613**, 743-750 (2023).
4. Ravens S, *et al.* Human gammadelta T cells are quickly reconstituted after stem-cell transplantation and show adaptive clonal expansion in response to viral infection. *Nat Immunol* **18**, 393-401 (2017).
5. Lien SC, *et al.* Tumor reactive gammadelta T cells contribute to a complete response to PD-1 blockade in a Merkel cell carcinoma patient. *Nat Commun* **15**, 1094 (2024).
6. von Borstel A, *et al.* Repeated Plasmodium falciparum infection in humans drives the clonal expansion of an adaptive gammadelta T cell repertoire. *Sci Transl Med* **13**, eabe7430 (2021).
7. Hunter S, *et al.* Human liver infiltrating gammadelta T cells are composed of clonally expanded circulating and tissue-resident populations. *J Hepatol* **69**, 654-665 (2018).
8. Kenna T, Golden-Mason L, Norris S, Hegarty JE, O'Farrelly C, Doherty DG. Distinct subpopulations of gamma delta T cells are present in normal and tumor-bearing human liver. *Clin Immunol* **113**, 56-63 (2004).
9. Wang X, *et al.* Host-derived lipids orchestrate pulmonary gammadelta T cell response to provide early protection against influenza virus infection. *Nat Commun* **12**, 1914 (2021).

10. Davey MS, *et al.* Clonal selection in the human V δ 1 T cell repertoire indicates gammadelta TCR-dependent adaptive immune surveillance. *Nat Commun* **8**, 14760 (2017).
11. Hoytema van Konijnenburg DP, Reis BS, Pedicord VA, Farache J, Victora GD, Mucida D. Intestinal Epithelial and Intraepithelial T Cell Crosstalk Mediates a Dynamic Response to Infection. *Cell* **171**, 783-794 e713 (2017).
12. Mayassi T, *et al.* Chronic Inflammation Permanently Reshapes Tissue-Resident Immunity in Celiac Disease. *Cell* **176**, 967-981 e919 (2019).
13. Li F, *et al.* The microbiota maintain homeostasis of liver-resident gammadeltaT-17 cells in a lipid antigen/CD1d-dependent manner. *Nat Commun* **7**, 13839 (2017).
14. Mangan BA, *et al.* Cutting edge: CD1d restriction and Th1/Th2/Th17 cytokine secretion by human V δ 3 T cells. *J Immunol* **191**, 30-34 (2013).
15. Russano AM, *et al.* Recognition of pollen-derived phosphatidyl-ethanolamine by human CD1d-restricted gamma delta T cells. *J Allergy Clin Immunol* **117**, 1178-1184 (2006).
16. Russano AM, *et al.* CD1-restricted recognition of exogenous and self-lipid antigens by duodenal gammadelta+ T lymphocytes. *J Immunol* **178**, 3620-3626 (2007).
17. Bai L, *et al.* The majority of CD1d-sulfatide-specific T cells in human blood use a semiinvariant V δ 1 TCR. *Eur J Immunol* **42**, 2505-2510 (2012).
18. Luoma AM, *et al.* Crystal structure of V δ 1 T cell receptor in complex with CD1d-sulfatide shows MHC-like recognition of a self-lipid by human gammadelta T cells. *Immunity* **39**, 1032-1042 (2013).
19. Uldrich AP, *et al.* CD1d-lipid antigen recognition by the gammadelta TCR. *Nat Immunol* **14**, 1137-1145 (2013).
20. Kenna T, *et al.* CD1 expression and CD1-restricted T cell activity in normal and tumour-bearing human liver. *Cancer Immunol Immunother* **56**, 563-572 (2007).
21. Wegrecki M, *et al.* Atypical sideways recognition of CD1a by autoreactive gammadelta T cell receptors. *Nat Commun* **13**, 3872 (2022).
22. Rice MT, *et al.* Recognition of the antigen-presenting molecule MR1 by a V δ 3(+) gammadelta T cell receptor. *Proc Natl Acad Sci U S A* **118**, e2110288118 (2021).
23. Le Nours J, *et al.* A class of gammadelta T cell receptors recognize the underside of the antigen-presenting molecule MR1. *Science* **366**, 1522-1527 (2019).

24. Borg NA, *et al.* CD1d-lipid-antigen recognition by the semi-invariant NKT T-cell receptor. *Nature* **448**, 44-49 (2007).
25. Reijneveld JF, *et al.* Human gammadelta T cells recognize CD1b by two distinct mechanisms. *Proc Natl Acad Sci U S A* **117**, 22944-22952 (2020).
26. Xin W, *et al.* Structures of human gammadelta T cell receptor-CD3 complex. *Nature* **630**, 222-229 (2024).
27. Hoque M, *et al.* Structural characterization of two gammadelta TCR/CD3 complexes. *Nat Commun* **16**, 318 (2025).
28. Franke D, Svergun DI. DAMMIF, a program for rapid ab-initio shape determination in small-angle scattering. *J Appl Crystallogr* **42**, 342-346 (2009).
29. Svergun DI. Restoring low resolution structure of biological macromolecules from solution scattering using simulated annealing. *Biophys J* **76**, 2879-2886 (1999).
30. Hopkins JB. BioXTAS RAW 2: new developments for a free open-source program for small-angle scattering data reduction and analysis. *J Appl Crystallogr* **57**, 194-208 (2024).
31. Le Nours J, *et al.* Atypical natural killer T-cell receptor recognition of CD1d-lipid antigens. *Nat Commun* **7**, 10570 (2016).
32. Gully BS, *et al.* Structure of a fully assembled gammadelta T cell antigen receptor. *Nature* **634**, 729-736 (2024).
33. Buresi C, Ghanem N, Huck S, Lefranc G, Lefranc MP. Exon duplication and triplication in the human T-cell receptor gamma constant region genes and RFLP in French, Lebanese, Tunisian, and black African populations. *Immunogenetics* **29**, 161-172 (1989).
34. Lameris R, *et al.* Enhanced CD1d phosphatidylserine presentation using a single-domain antibody promotes immunomodulatory CD1d-TIM-3 interactions. *J Immunother Cancer* **11**, e007631 (2023).
35. Huang S, *et al.* CD1 lipidomes reveal lipid-binding motifs and size-based antigen-display mechanisms. *Cell* **186**, 4583-4596 e4513 (2023).
36. Sok CL, Rossjohn J, Gully BS. The Evolving Portrait of gammadelta TCR Recognition Determinants. *J Immunol* **213**, 543-552 (2024).

37. Gully BS, Rossjohn J, Davey MS. Our evolving understanding of the role of the gammadelta T cell receptor in gammadelta T cell mediated immunity. *Biochem Soc Trans* **49**, 1985-1995 (2021).
38. Lameris R, *et al.* A single-domain bispecific antibody targeting CD1d and the NKT T-cell receptor induces a potent antitumor response. *Nat Cancer* **1**, 1054-1065 (2020).
39. Birkinshaw RW, *et al.* alphabeta T cell antigen receptor recognition of CD1a presenting self lipid ligands. *Nat Immunol* **16**, 258-266 (2015).
40. Wun KS, *et al.* T cell autoreactivity directed toward CD1c itself rather than toward carried self lipids. *Nat Immunol* **19**, 397-406 (2018).
41. Cotton RN, *et al.* CD1a selectively captures endogenous cellular lipids that broadly block T cell response. *J Exp Med* **218**, e20202699 (2021).
42. Cheng TY, *et al.* Lipidomic scanning of self-lipids identifies headless antigens for natural killer T cells. *Proc Natl Acad Sci U S A* **121**, e2321686121 (2024).
43. Kjer-Nielsen L, *et al.* A structural basis for selection and cross-species reactivity of the semi-invariant NKT cell receptor in CD1d/glycolipid recognition. *J Exp Med* **203**, 661-673 (2006).
44. Aragao D, *et al.* MX2: a high-flux undulator microfocus beamline serving both the chemical and macromolecular crystallography communities at the Australian Synchrotron. *J Synchrotron Radiat* **25**, 885-891 (2018).
45. Adams PD, *et al.* The Phenix software for automated determination of macromolecular structures. *Methods* **55**, 94-106 (2011).
46. Emsley P, Lohkamp B, Scott WG, Cowtan K. Features and development of Coot. *Acta Crystallogr D Biol Crystallogr* **66**, 486-501 (2010).
47. Krissinel E, Henrick K. Inference of macromolecular assemblies from crystalline state. *J Mol Biol* **372**, 774-797 (2007).
48. Kirby N, *et al.* Improved radiation dose efficiency in solution SAXS using a sheath flow sample environment. *Acta Crystallogr D Struct Biol* **72**, 1254-1266 (2016).
49. Svergun D, Barberato, C. and Koch, M. H. J. . CRYSTOL - a Program to Evaluate X-ray Solution Scattering of Biological Marcomolecules from Atmoic Coordinates. *Journal of Applied Crystallography* **28**, 768-773 (1995).

ARTICLE IN PRESS

Figure Legends

Figure 1: CD1d recognition by V δ 1+ $\gamma\delta$ TCRs. (A) Affinity measurement analysis of $\gamma\delta$ TCRs 2, 3 and 6, 7, 8 and the $\alpha\beta$ NKT TCR determined by SPR. Sensograms are representative of a single dilution series. Error bars denote S.E.M., K_D was determined from two independent experiments, performed in duplicate, using a 1:1 binding model. (B) SEC-SAXS analysis of $\gamma\delta$ TCRs co-complexed with CD1d with *ab initio* models aligned with the 9C2 $\gamma\delta$ TCR-CD1d complex or individual TCR and CD1d components. The 9C2 $\gamma\delta$ chains were coloured in light and dark red respectively, CD1d dark grey, β_2 M in black and the *ab initio* reconstruction shown in white.

Figure 2: CD1d activates $\gamma\delta$ T cells. (A) Mean Fluorescence Index (MFI) of $\gamma\delta$ TCR transduced Jurkat.76 cells after 16 co-culture with K562.WT and K562.CD1d cells assessing CD69 upregulation and CD3 downregulation. Significance is comparing Baseline, Jurkat cells alone to co-culture. Data was generated from two independent experiments, performed in duplicate. (B) CD69 and CD3 MFI following serial dilution of α -GalCer with K562.CD1d cells, assessing CD69 and CD3 levels compared to vehicle, 0 μ M of α -GalCer with K562 CD1d cells. Data was generated from two independent experiments, performed in duplicate. (C) Jurkat T cell Nur77 MFI and Frequency was assessed following 2 hours of co-culture with either K562 WT or CD1d cells. Data was generated from three independent experiments, performed in duplicate. Statistical analysis was performed with one-way ANOVA with Tukey's multiple comparison test. Error bars denote S.E.M.

Figure 3. CD1d-induced TCR clustering and CD3 phosphorylation. *d*STORM images of CD1d-reactive $\alpha\beta$ TCR 9C1 and CD1d-reactive $\gamma\delta$ TCRs expressed in Jurkat T cells, stimulated with ICAM-1 alone, ICAM-1 + CD1d-endo (A) or ICAM-1 + CD1d- α -GalCer (B) on supported lipid bilayers (SLBs) at varying concentrations. Cells were stained for CD3 (AF647, red) and CD3 ζ /pCD3 ζ (AF568, green). ICAM-1-only SLBs served as antigen-free unstimulated controls. Scale bar: 5 μ m. (C and D) Cluster analysis of *d*STORM images using DBSCAN and Clus-DoC. DBSCAN and Clus-DoC Analysis was performed across $n \geq 30$ single Jurkat T cells with three

independent replicates. Statistical analysis was performed using one-way ANOVA with Tukey's multiple comparisons test against ICAM-1 controls. Error bars represent S.E.M.

Figure 4: Impact of C γ Exon 2 insertions upon $\gamma\delta$ T cell activation. (A) MFI of CD69 and CD3 of 9C2 $\gamma\delta$ TCR C γ alleles transduced into Jurkat cells. Activation was measured following co-culture with either K562.WT or K562.CD1d cells after 16 hours of stimulation. (B) Assessment of Jurkat T cells CD69 and CD3 surface expression post 16-hour stimulation with K562.CD1d cells treated with dilutions of α -GalCer. (C) *d*STORM images of 9C2 C γ alleles stimulated with ICAM-1, ICAM-1 + CD1d-endo or ICAM-1 + CD1d- α GalCer. Cells were stained with α -CD3 (red) and α -CD3 ζ /p-CD3 ζ (green). Cluster analysis of CD1d-endo (D) and CD1d- α GalCer (E) stimulated cells. Analysis was performed as outlined in Figure 3, using one-way ANOVA with Tukey's multiple comparison test. Analysis was performed on two independent experiments, with duplicate wells. Error bars denote S.E.M.

Figure 5: Structural overview of the $\gamma\delta$ TCR-CD1d complex. Cartoon representation of $\gamma\delta$ TCR-2 bound to CD1d-‘endo’(A), 9C2 $\gamma\delta$ TCR bound to CD1d-‘ α -GalCer’(B)(PDB ID: 4LHU) and DP10.7 $\gamma\delta$ TCR bound to CD1d-‘sulfatide’ (C)(PDB ID: 4MNG). TCR γ/δ chains are coloured light/dark variants of blue, red and green. CD1d is shown in grey, β_2 M in black. CDR loop positions and V chain COM shown for $\gamma\delta$ TCR-2 (D), 9C2 (E) and DP10.7 (F). V δ and V γ COM are coloured in black and white respectively. CDR loops are coloured pink-CDR1 γ , orange-CDR2 γ , purple-CDR3 γ , red-FW γ , yellow-CDR1 δ , green-CDR2 δ , blue-CDR3 δ and light-blue-FW δ . FW denotes framework contacts. Molecular contacts on CD1d shown for $\gamma\delta$ TCR-2 (G), 9C2 (H) and DP10.7 (I), coloured as seen in (D-F). Lipid antigens are either depicted as sticks (A-F) or spheres (G-I).

Figure 6 : Molecular interface of the $\gamma\delta$ TCR 2 CD1d interaction. (A) Buried Surface Area and CDR loop contributions of the $\gamma\delta$ TCR 2-CD1d interface. Interactions between $\gamma\delta$ TCR 2 and CD1d via FW γ , CDR1 γ and CDR2 γ (B), CDR3 γ (C) and CDR1 δ , CDR3 δ (D). CDR loops are coloured pink-CDR1 γ , orange-CDR2 γ , purple-CDR3 γ , red-FW γ , yellow-CDR1 δ , green-CDR2 δ and blue-CDR3 δ . FW denotes framework contacts. CD1d is shown in dark grey. Sphingomyelin

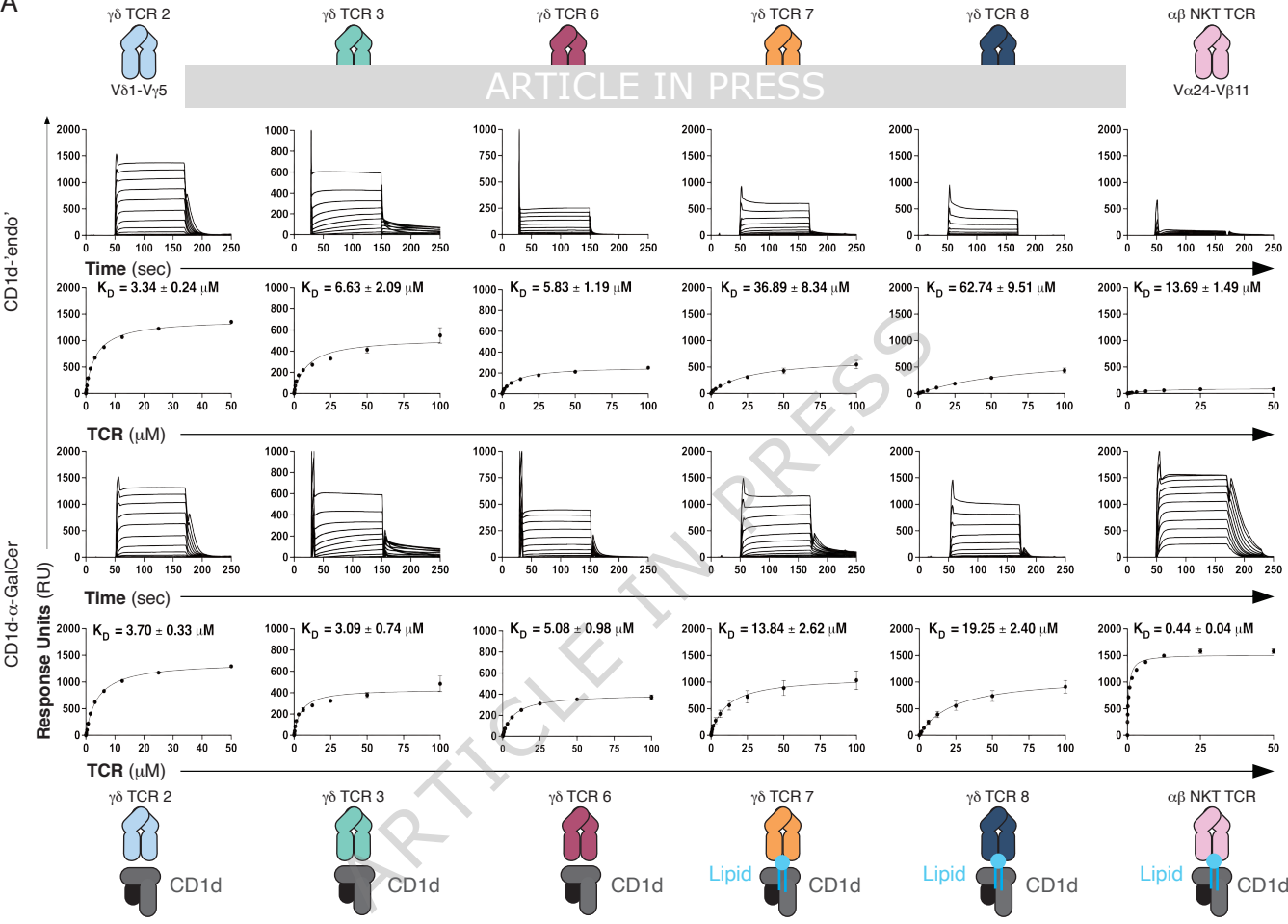
lipid is shown as sticks. Dotted lines denote hydrogen bonds, parentheses indicate Van der Waals interactions.

Editorial Summary

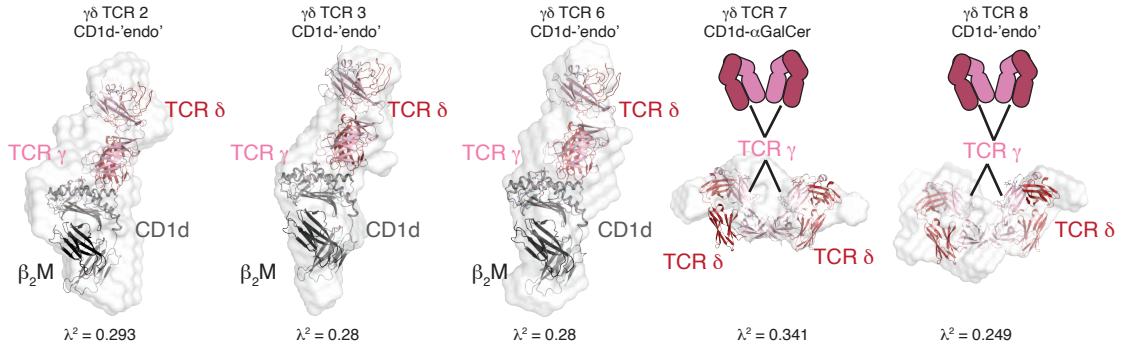
T cells can recognise lipid antigen in the context of CD1d molecules. Here, the authors show that $\gamma\delta$ T cell activation in response to CD1d differs from that of $\alpha\beta$ T cells and determine the structure of a $\gamma\delta$ T cell receptor that binds to CD1d independently of the presented lipid.

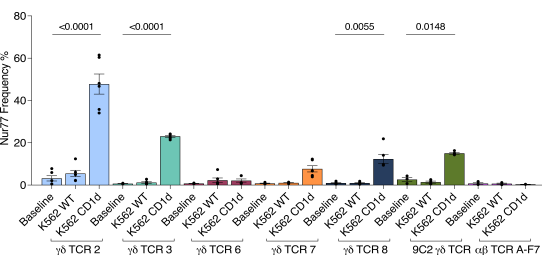
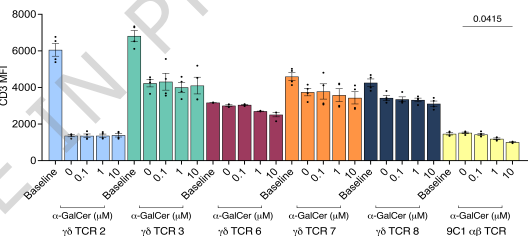
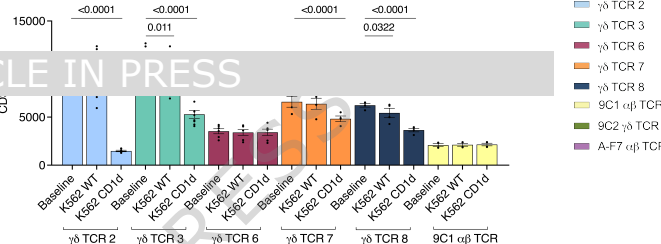
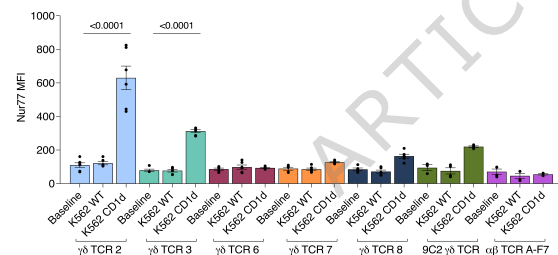
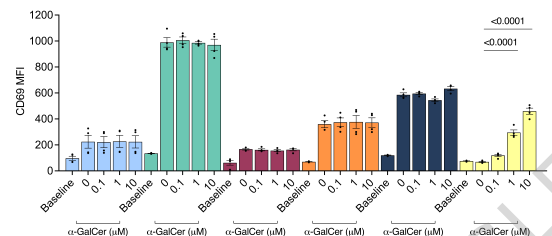
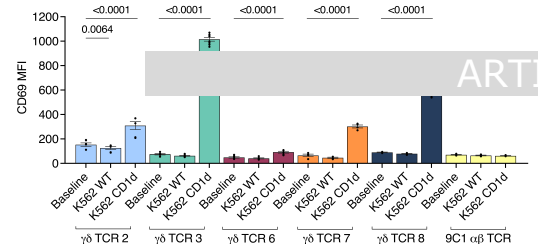
Peer Review Information: *Nature Communications* thanks Laurent Gapin, Salah Mansour and Lawrence Stern for their contribution to the peer review of this work. A peer review file is available.

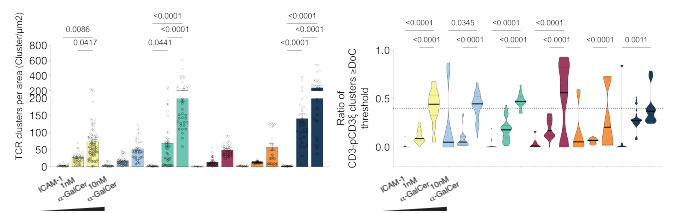
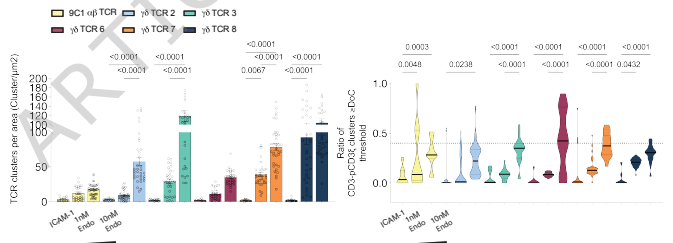
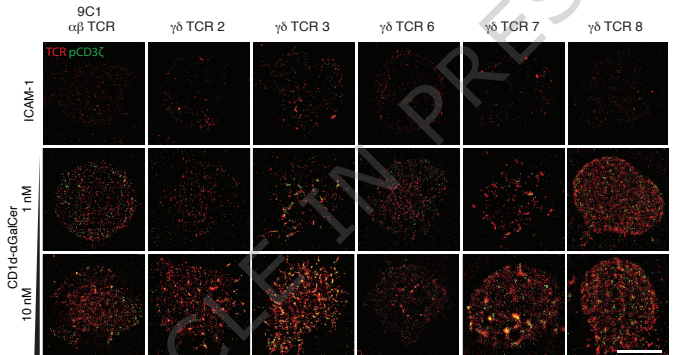
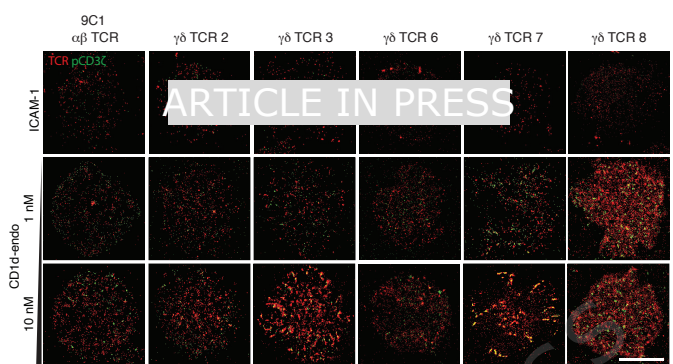
A

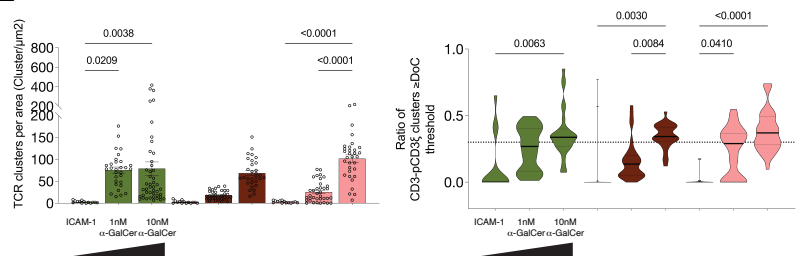
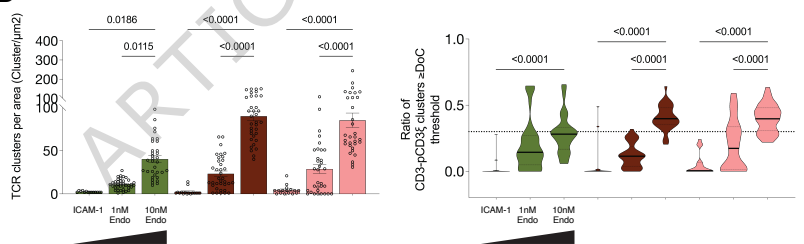
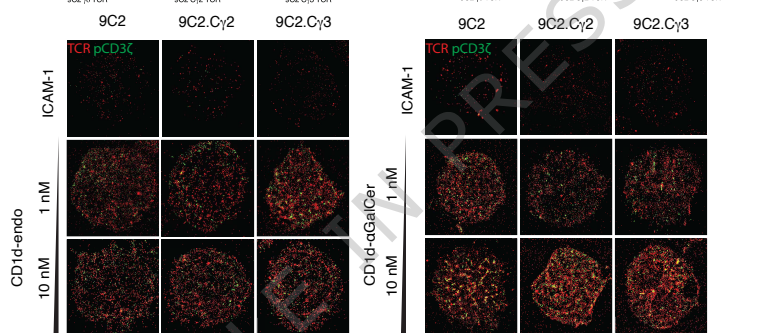
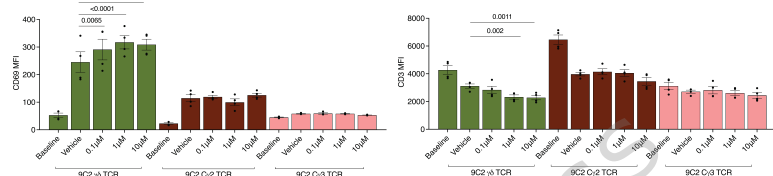
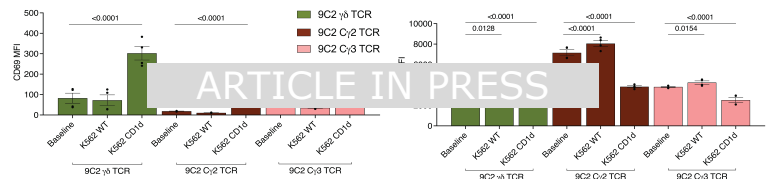


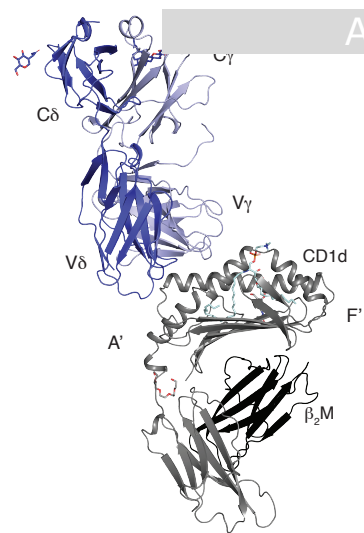
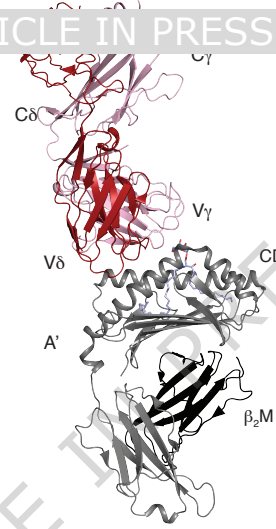
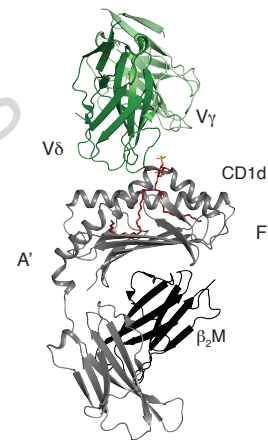
B



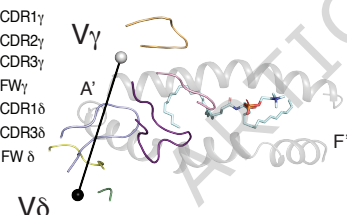
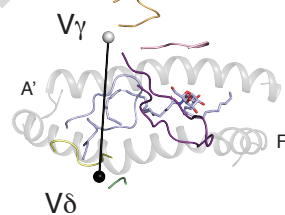
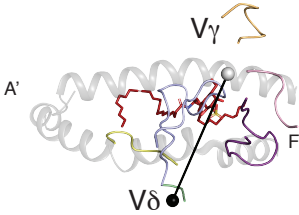
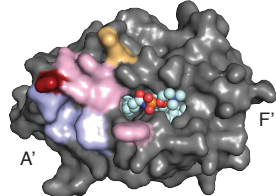
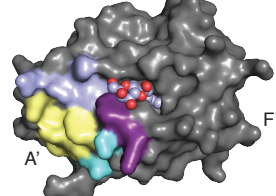
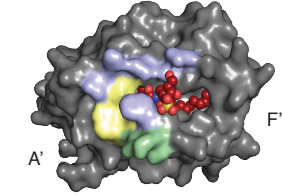






A $\gamma\delta$ TCR-2 CD1d-'endo'**B**9C2 $\gamma\delta$ TCR CD1d-' α -GalCer'**C**DP10.7 $\gamma\delta$ TCR CD1d-'sulfatide'**D**

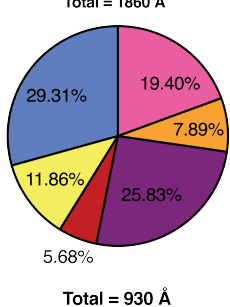
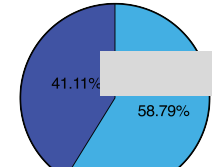
- CDR1 γ
- CDR2 γ
- CDR3 γ
- FW γ
- CDR1 δ
- CDR3 δ
- FW δ

**E****F****G****H****I**

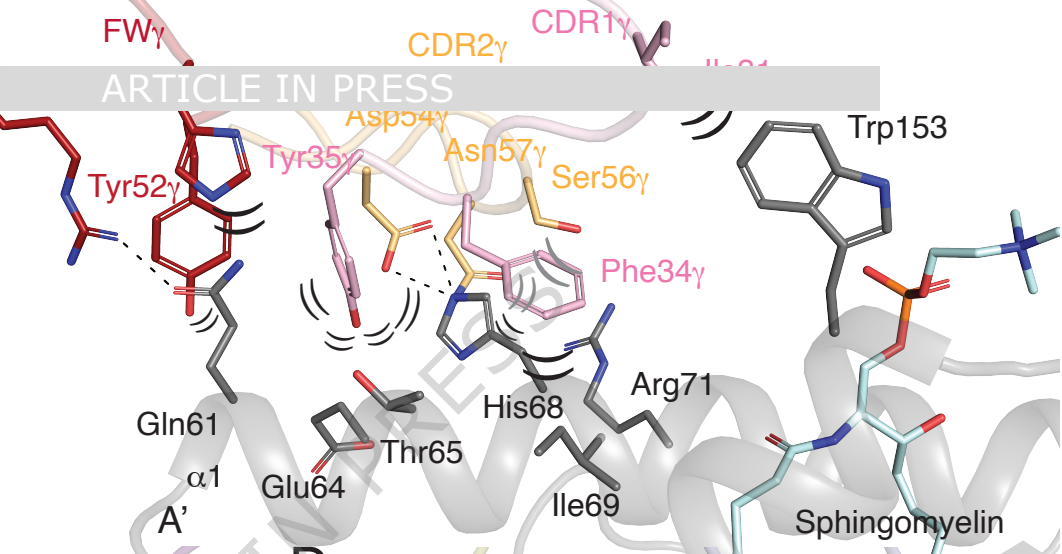
A

B

ARTICLE IN PRESS



█ CDR1 γ
█ CDR2 γ
█ CDR3 γ
█ FWy
█ CDR1 δ
█ CDR3 δ



C

